A LETTERS JOURNAL EXPLORING THE FRONTIERS OF PHYSICS

OFFPRINT

Analysis and manufacture of an energy harvester based on a Mooney-Rivlin–type dielectric elastomer

YANJU LIU, LIWU LIU, ZHEN ZHANG, YANG JIAO, SHOUHUA SUN and JINSONG LENG

EPL, **90** (2010) 36004

epl A Letters Journal Exploring the Frontiers of Physics

May 2010

EPL, **90** (2010) 36004
doi: 10.1209/0295-5075/90/36004

www.epljournal.org

Analysis and manufacture of an energy harvester based on a Mooney-Rivlin–type dielectric elastomer

Yanju Liu[1(a)], Liwu Liu[1], Zhen Zhang[2], Yang Jiao[1], Shouhua Sun[1] and Jinsong Leng[2(b)]

[1] *Department of Astronautical Science and Mechanics, Harbin Institute of Technology (HIT) - P.O. Box 301, No. 92 West Dazhi Street, Harbin 150001, PRC*
[2] *Centre for Composite Materials, Science Park of Harbin Institute of Technology (HIT) - P.O. Box 3011, No. 2 YiKuang Street, Harbin 150080, PRC*

received 3 October 2009; accepted in final form 26 April 2010
published online 28 May 2010

PACS 61.41.+e – Polymers, elastomers, and plastics
PACS 77.84.Jd – Polymers; organic compounds
PACS 77.65.-j – Piezoelectricity and electromechanical effects

Abstract – We studied a typical failure model of a Mooney-Rivlin–type silicone energy harvester, illustrated the allowable area under equal-biaxial and unequal-biaxial conditions, calculated the energy generated in one cycle of an energy harvester, designed a new harvester, and conducted its primary tests. When the ratio between principal planar stretches $p = 1$ ($\lambda_2 = p\lambda_1$) and the material constant ratio $k = 0.1$ ($C_2 = kC_1$), the energy density generated by the harvester is 6.81 J/g. We think that these results can be used to facilitate the design and manufacture of dielectric elastomer energy harvesters.

Silicone dielectric elastomer (DE) is generally regarded as a type of electroactive polymer (EAP) material with many applications in active actuator, sensor and energy harvester [1–8], because of its unique advantages such as large deformation, little response time, high elastic energy density, high efficiency, and long fatigue lifespan [1–3]. The film thins down and expands in area after a voltage is applied on a dielectric elastomer sandwiched by compliant electrodes [1–3,9]. Numerous actuators (plane actuator, rolled actuator, hemisphere actuator, folded actuators and staking actuator) and sensors can be designed based on this principle [2]. The inspirations were also demonstrated by experiments [2,3].

The basic principle of an energy harvester based on dielectric elastomer can be expressed as follows: an electric charge is placed on an electrode, when a pre-stretch is applied to a dielectric elastomer membrane. The pre-stretch is generated by applying a mechanical force to the side of a membrane. As the result of pre-stretch, the membrane becomes thinner in thickness, and its capacitance increases, and mechanical energy is thus converted into elastic energy. After the mechanical force is removed, because of elasticity, the thickness of the membrane increases while its capacitance decreases, and elastic energy is thus converted into electrical energy. A complete cycle of conversion from elastic energy to electric energy is thus accomplished. Piezoelectric materials can also be used to fabricate the energy harvester based on the above-mentioned basic principle, and the theoretical investigations have been analyzed extensively by using the models as follows [9–16].

The electromechanical stability of a dielectric elastomer and its actuator has been delved for some years [17–38], however, the theoretical research on a dielectric elastomer generator is just beginning [17]. Koh *et al.* obtained the allowable area of an energy harvester based on neo-Hookean model [17]. They calculated the maximal energy generated by the harvester in one cycle.

In this paper, we studied the typical failure model of a Mooney-Rivlin silicone energy harvester, derived the constitutive relationship of a silicone elastomer under the coupling of electric and mechanical fields. We calculated the allowable area of an energy harvester under equal-biaxial and unequal-biaxial conditions. Based on these calculations, we designed a dielectric-elastomer–based energy harvester and evaluated its performance.

Pure silicone is a typical Mooney-Rivlin soft material, its elastic strain energy function $W(I_1, I_2, I_3)$ depends on the deformation gradient, $F_{iK}(X,t) = \partial x_i(X,t)/\partial X_K$,

(a) E-mail: yj_liu@hit.edu.cn
(b) E-mail: lengjs@hit.edu.cn

where I_1, I_2, I_3 are left Cauchy-Green deformation tensor, $I_1 = F_{iK}F_{iK}$, $I_2 = [F_{iK}F_{iK}F_{jM}F_{jM} - F_{iK}F_{jK}F_{iM}F_{jM}]/2$ and $I_3 = \det\{F_{iK}F_{jK}\}$.

The deformation of the arbitrary mass point X in the current state and at time t can be denoted by $x_i(X,t)$. Considering the simple process of tension, the lengths in the three principal directions in the reference state can be assumed to be L_1, L_2 and L_3, respectively, and the lengths in the current state can be expressed as l_1, l_2 and l_3, respectively. The stretches in the three principal directions can thus be $\lambda_1 = l_1/L_1$, $\lambda_2 = l_2/L_2$ and $\lambda_3 = l_3/L_3$, respectively. Then the left Cauchy-Green deformation tensor can be simplified by taking into account the assumption of incompressibility, $I_1 = \lambda_1^2 + \lambda_2^2 + \lambda_1^{-2}\lambda_2^{-2}$, $I_1 = \lambda_1^2 + \lambda_2^2 + \lambda_1^{-2}\lambda_2^{-2}$ and $I_3 = \lambda_1^2\lambda_2^2\lambda_3^2 = 1$.

Subjected to the electric voltage U, each surface of the silicone rubber gains a magnitude of electric charge Q. The nominal electric field can be denoted by $E^{\sim} = U/L_3$ and the corresponding true electric field is $E = U/l_3 = U/\lambda_3 L_3$. The nominal electric displacement is $D^{\sim} = Q/L_1L_2$ and the corresponding true electric displacement is $D = Q/l_1l_2 = Q/\lambda_1L_1\lambda_2L_2$.

The elastic strain energy function of silicone DE can be expressed as the Mooney-Rivlin model

$$W(I_1, I_2) = \sum_{\alpha,\beta\geqslant 0} C_{\alpha\beta}(I_1-3)^{\alpha}(I_2-3)^{\beta}, \tag{1}$$

where $D^{\sim}$ is the nominal electric displacement, and ε is the permittivity of the silicone rubber.

We can then get the nominal stress and nominal electric field of an electromechanical coupling system based on a silicone dielectric elastomer as shown below:

$$s_i = \sum_{\alpha,\beta\geqslant 0} C_{\alpha\beta}\left[\alpha(I_1-3)^{\alpha-1}(I_2-3)^{\beta}\frac{\partial I_1}{\partial\lambda_i} + \beta(I_2-3)^{\beta-1}\,(I_1-3)^{\alpha}\frac{\partial I_2}{\partial\lambda_i}\right] - \frac{D^{\sim 2}}{\varepsilon}\lambda_i^{-1}\lambda_1^{-2}\lambda_2^{-2}, \tag{2a}$$

$$E^{\sim} = \frac{\partial W}{\partial D^{\sim}} = \frac{D^{\sim}}{\varepsilon}\lambda_1^{-2}\lambda_2^{-2}. \tag{2b}$$

From the relations given above, the true stresses can be written as $\sigma_1 = s_1\lambda_1$, $\sigma_2 = s_2\lambda_2$. By substituting them into (2a) and (2b), the corresponding true nominal stress and true nominal electric field of the silicone rubber dielectric elastomer are, respectively,

$$\sigma_i = \sum_{\alpha,\beta\geqslant 0} C_{\alpha\beta}\left[\alpha(I_1-3)^{\alpha-1}(I_2-3)^{\beta}\frac{\partial I_1}{\partial\lambda_i} + \beta(I_2-3)^{\beta-1}(I_1-3)^{\alpha}\frac{\partial I_2}{\partial\lambda_i}\right]\lambda_i - \frac{D^{\sim 2}}{\varepsilon}\lambda_1^{-2}\lambda_2^{-2}, \tag{3a}$$

$$E = \frac{D}{\varepsilon}. \tag{3b}$$

By taking eq. (1) into account, the Mooney-Rivlin model can be simplified into an elastic strain energy function with two material constants. By setting $\alpha = 1$, $\beta = 0$, $\alpha = 0$, $\beta = 1$, $C_1 = 2C_{10}$ and $C_2 = 2C_{01}$, under the equal-biaxial condition $\lambda_1 = \lambda_2 = \lambda$ and $C_2 = kC_1$ (k is the material constant ratio), due to the dielectric elastomer's incompressibility, we get $\lambda_3 = \lambda^{-2}$, and the free energy can be described as

$$W(\lambda, D^{\sim}) = \frac{C_1}{2}(2\lambda^2 + \lambda^{-4} - 3) + \frac{kC_1}{2}(2\lambda^{-2} + \lambda^4 - 3) + \frac{D^{\sim 2}}{2\varepsilon}\lambda^{-4}. \tag{4}$$

Evidently, the condition in which the material constant $k = 0$ has been studied by Koh *et al.* [17].

Considering eqs. (1) and (4), the relations between nominal stress and stretch, nominal electric field and nominal electric displacement can be listed as shown below:

$$\frac{s}{C_1} = 2\lambda - 2\lambda^{-5} + 2k(\lambda^3 - \lambda^{-3}) - \frac{2D^{\sim 2}}{C_1\varepsilon}\lambda^{-5}, \tag{5a}$$

$$\frac{E^{\sim}}{\sqrt{C_1/\varepsilon}} = \frac{D^{\sim}}{\sqrt{C_1\varepsilon}}\lambda^{-4}. \tag{5b}$$

The condition of zero-field stress-strain is simply to satisfy the fundamental thermodynamic stability. The failure process can be simplified, namely $D^{\sim} = 0$ and $E^{\sim} = 0$. From eq. (5), we have the first critical condition for the allowable area as shown below:

$$\frac{s}{C_1} = 2\lambda - 2\lambda^{-5} + 2k(\lambda^3 - \lambda^{-3}). \tag{6}$$

The second critical condition for allowable area can be defined as electrical breakdown. For a soft active dielectric elastomer, the elastomer will be broken down when the exerted static electric field goes beyond the critical breakdown point of an electric field. The static breakdown strength can be measured through experiments. Here we take a typical value $E_{EB} = 3\times 10^8\,\mathrm{V/m}$ [1,17], and C_1 and ε are typical values, respectively, namely $C_1 = 1\times 10^6\,\mathrm{N/m^2}$ [18] and $\varepsilon = 3.54\times 10^{-11}\,\mathrm{F/m}$ [27].

$$\frac{s}{C_1} = 2\lambda - 2\lambda^{-5} + 2k(\lambda^3 - \lambda^{-3}) - \frac{2E_{EB}^2}{C_1/\varepsilon}\lambda^{-1}, \tag{7a}$$

$$\frac{E^{\sim}}{\sqrt{C_1/\varepsilon}} = \frac{E_{EB}^2}{C_1/\varepsilon}\left(\frac{D^{\sim}}{\sqrt{C_1\varepsilon}}\right)^{-1}. \tag{7b}$$

The third condition for the allowable area is based on the consideration of electromechanical instability (EMI) [17,27,35]. A dielectric elastomer film under pre-stretch load will expand in the film plane and shrink along the thickness direction when a mechanical force field and an electric field are applied. Such changes cause a high electric field in the dielectric elastomer, which results in a positive feedback loop. If the positive feedback process continues, the dielectric elastomer film will break down when the critical electric field is reached. From eq. (5),

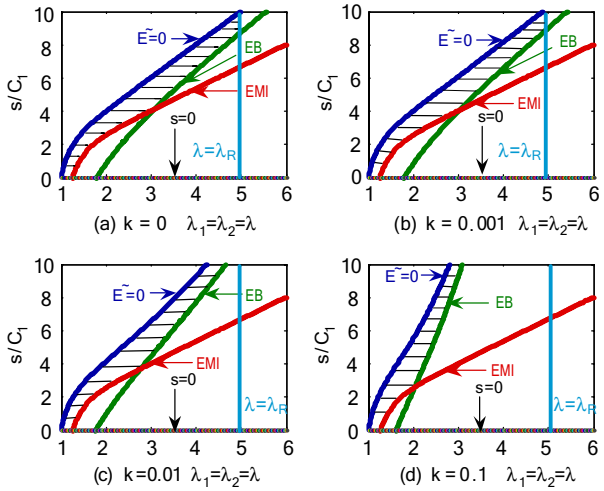

Fig. 1: (Color online) Relation between deformation and stress of a Mooney-Rivlin–type DE generator when $\lambda_1=\lambda_2=\lambda$ (hatching representing the allowable area).

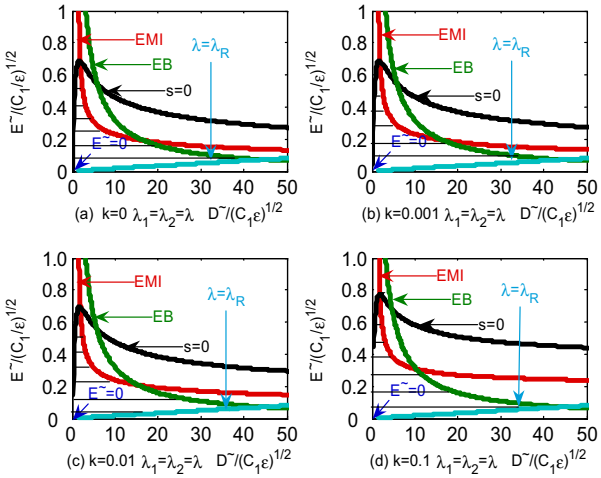

Fig. 2: (Color online) Relation between nominal electric field and nominal electric displacement of various Mooney-Rivlin–type DE generators when $\lambda_1=\lambda_2=\lambda$ (hatching representing the allowable area).

$$s/C_1=4(\lambda-4\lambda^{-5}-3k\lambda^{-3})/3,$$

$$\frac{D^{\sim}}{\sqrt{C_1\varepsilon}}=\sqrt{\frac{1}{3}(\lambda^6+5)+k(\lambda^8+\lambda^2)}, \tag{8a}$$

$$\frac{E^{\sim}}{\sqrt{C_1/\varepsilon}}=\lambda^{-4}\sqrt{\frac{1}{3}(\lambda^6+5)+k(\lambda^8+\lambda^2)}. \tag{8b}$$

The following energy harvester failure model can be called as tension loss, which leads to the formation of wrinkles, and results in a premature electrical breakdown [39]. For example, without pre-stretching, the rolling actuator based on dielectric elastomer cannot work [2]. Moreover, it has been confirmed using various experiments and theories that can be enhanced by the stability of a dielectric elastomer [1,18,29]. When the tension loses, namely $s=0$, the relation between nominal electric field and nominal displacement in the DE generator can be established as shown below:

$$\frac{D^{\sim}}{\sqrt{C_1\varepsilon}}=\sqrt{\lambda^6-1+k(\lambda^8-\lambda^2)}, \tag{9a}$$

$$\frac{E^{\sim}}{\sqrt{C_1/\varepsilon}}=\lambda^{-4}\sqrt{\lambda^6-1+k(\lambda^8-\lambda^2)}. \tag{9b}$$

What is shown by the following failure model is the case of damage to the dielectric elastomer film. For an ideal dielectric elastomer, the stretch in the planar direction is: $\lambda_1\leqslant 5$, and $\lambda_2\leqslant 5$ [27,28]. When a generator fails, the stretch reaches a critical value in the planar direction, $\lambda_R=5$,

$$\frac{E^{\sim}}{\sqrt{C_1/\varepsilon}}=\frac{D^{\sim}}{\sqrt{C_1\varepsilon}}\lambda_R^{-4}. \tag{10}$$

We synthesized control equations (6)–(10), and gave the allowable area of the Mooney-Rivlin–type DE generator under planar biaxial and equal tensile loads with different constants k. As shown in figs. 1 and 2, when $k=0$, the allowable area obtained through our calculation is identical to what is shown in the conclusion of Koh *et al.* [17].

The equal-biaxial experiment is common, see, for instance, the apex of an inflating membrane, and an expanding balloon [36,38,40]. However, what we need in many cases is the biaxial stretching in accordance with the specific ratio between the two axes. Hence the unequal-biaxial condition is considered. Let $\lambda_2=p\lambda_1$ with $p>0$, which is the ratio between the principal planar stretches and $p=1$ means the equal-biaxial condition. To simplify the formulation, let $\lambda_1=\lambda$, similar to the processing method mentioned above. We have the following free-energy function of the dielectric elastomer:

$$W(\lambda,D^{\sim})=\frac{C_1}{2}[(1+p^2)\lambda^2+p^{-2}\lambda^{-4}-3]+\frac{kC_1}{2}[(1+p^{-2})\lambda^{-2}+p^2\lambda^4-3]+\frac{D^{\sim 2}}{2\varepsilon}p^{-2}\lambda^{-4}. \tag{11}$$

According to the processing method mentioned above, the typical failure models of dielectric elastomers are separately taken into account: in sequence, disappearance electric charge, static electric breakdown, electromechanical instability, disappearance tension and stretch damage. Then, we deduced the governing equations for the stable allowable areas as shown below.

$$\begin{cases}\dfrac{s}{C_1}=(1+p^2)\lambda-2p^{-2}\lambda^{-5}+2kp^2\lambda^3-k(1+p^{-2})\lambda^{-3},\\ \dfrac{s}{C_1}=(1+p^2)\lambda-2p^{-2}\lambda^{-5}+2kp^2\lambda^3-k(1+p^{-2})\lambda^{-3}\\ \qquad -\dfrac{2p^{-2}E_{EB}^2}{C_1/\varepsilon}\lambda^{-1},\\ \dfrac{s}{C_1}=\dfrac{2(1+p^2)\lambda-16p^{-2}\lambda^{-5}-6k(1+p^{-2})\lambda^{-3}}{3},\\ \dfrac{s}{C_1}=0,\\ \dfrac{s}{C_1}\geqslant 0,\quad \lambda_R=5,\end{cases} \tag{12a}$$

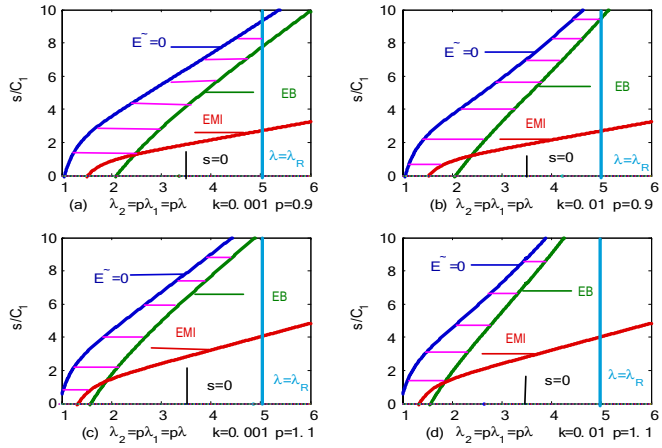

Fig. 3: (Color online) Relation between deformation and stress of a Mooney-Rivlin–type DE generator when $\lambda_2 = p\lambda_1 = p\lambda$ and $k = 0.001, 0.01$ (hatching representing the allowable area).

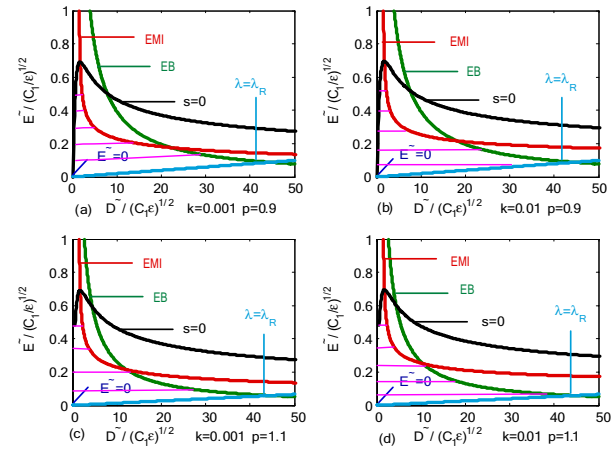

Fig. 4: (Color online) Relation between nominal electric field and nominal electric displacement of a Mooney-Rivlin–type DE generator when $\lambda_2 = p\lambda_1 = p\lambda$ and $k = 0.001, 0.01$ (hatching representing the allowable area).

$$
\begin{cases}
\dfrac{E^{\sim}}{\sqrt{C_1/\varepsilon}} = 0, \quad \dfrac{D^{\sim}}{\sqrt{C_1\varepsilon}} = 0, \\
\dfrac{E^{\sim}}{\sqrt{C_1/\varepsilon}} = p^{-2}\dfrac{E_{EB}^2}{C_1/\varepsilon}\left(\dfrac{D^{\sim}}{\sqrt{C_1\varepsilon}}\right)^{-1}, \quad 0 < \dfrac{D^{\sim}}{\sqrt{C_1\varepsilon}} \leqslant 50, \\
\dfrac{E^{\sim}}{\sqrt{C_1/\varepsilon}} = \dfrac{D^{\sim}}{\sqrt{C_1\varepsilon}}p^{-2}\lambda^{-4}, \\
\dfrac{D^{\sim}}{\sqrt{C_1\varepsilon}} = \sqrt{\dfrac{p^2(p^2+1)\lambda^6 + 10 + 6kp^4\lambda^8 + 3k(p^2+1)\lambda^2}{6}}, \\
\dfrac{E^{\sim}}{\sqrt{C_1/\varepsilon}} = \dfrac{D^{\sim}}{\sqrt{C_1\varepsilon}}p^{-2}\lambda^{-4}, \\
\dfrac{D^{\sim}}{\sqrt{C_1\varepsilon}} = \sqrt{\dfrac{p^2(p^2+1)\lambda^6 - 2 + 2kp^4\lambda^8 - k(p^2+1)\lambda^2}{2}}, \\
\dfrac{E^{\sim}}{\sqrt{C_1/\varepsilon}} = \dfrac{D^{\sim}}{\sqrt{C_1\varepsilon}}p^{-2}\lambda_R^{-4}, \quad \lambda_R = 5, \quad 0 < \dfrac{D^{\sim}}{\sqrt{C_1\varepsilon}} \leqslant 50.
\end{cases}
\tag{12b}
$$

As shown in figs. 3 and 4, the allowable area decreases with the increase of the ratio between principal planar stretches and with the increase of the material constant ratio k as well. According to eq. (12), when $p > 0.45$, the nominal stress $s > 0$ and the nominal electric displacement $D^{\sim} > 0$ (equivalent to $E^{\sim} > 0$). To design a harvester with a larger allowable working area, the values of the parameters p and k should be small. For example, the EMI curve moves upward in the plane formed by the nominal electric field and so the allowable area increases as p decreases.

The hatched part in fig. 5 represents the working cycle of an energy harvester, which can be used to calculate the energy density ξ generated by the harvester in one cycle. That is $\xi = [\rho X_2(Y_3 - Y_2)]/C_1$, in which $\rho = 1000\,\mathrm{kg/m^3}$

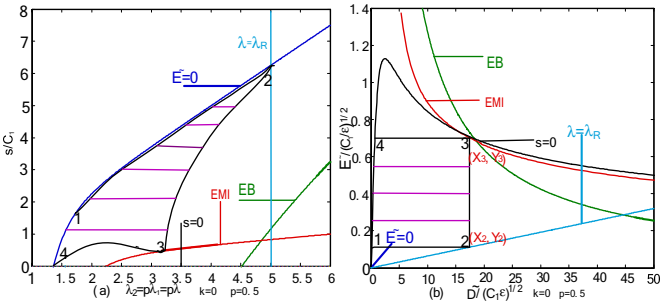

Fig. 5: (Color online) (a) Deformation and stress, (b) nominal electric field and nominal electric displacement of a Mooney-Rivlin–type DE generator when $\lambda_2 = 0.5\lambda_1 = 0.5\lambda$ and $k = 0$ (hatching represents the energy generated in one cycle).

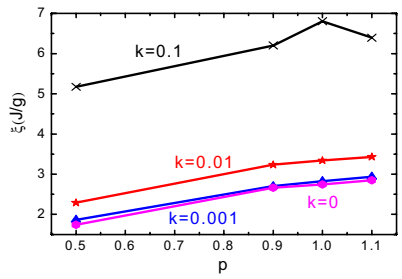

Fig. 6: (Color online) Energy density of the energy harvester for different values of p and k.

is the density of an elastic body and X_2, Y_2, X_3 and Y_3 are the coordinates of points 2 and 3 in fig. 5(b). If X_2 is known, then $\xi = \frac{\rho}{C_1}X_2^2 p^{-2}(\lambda_{(3)}^{-4} - \frac{1}{625})$ and $\lambda_{(3)}$ satisfies the following equation:

$$
X_2 = \sqrt{\frac{p^2(p^2+1)\lambda_{(3)}^6 + 10 + 6kp^4\lambda_{(3)}^8 + 3k(p^2+1)\lambda_{(3)}^2}{6}}.
$$

$$\xi = \begin{cases} \dfrac{\rho[6kp^2\lambda_{\xi1}^8 + (p^2+3kp^{-2}+1+3k)\lambda_{\xi1}^6 + 10p^{-2}]\left(\lambda_{\xi1}^{-4} - \dfrac{1}{625}\right)}{6C_1}, & 1 \leqslant \lambda_{\xi1} \leqslant \lambda_{EMI=EB}, \\ \dfrac{\rho[2kp^2\lambda_{\xi2}^8 + (p^2+1)\lambda_{\xi2}^6 - k(1+p^{-2})\lambda_{\xi2}^2 - 2p^{-2}]\left(\lambda_{\xi2}^{-4} - \dfrac{1}{625}\right)}{2C_1}, & \lambda_{EMI=EB} < \lambda_{\xi2} \leqslant \lambda_R, \end{cases} \tag{13a}$$

It is proved through further investigation that the maximum energy ξ generated by a harvester in a single work cycle is

see eq. (13a) *above*

$\lambda_{\xi1}$ and $\lambda_{\xi2}$ in eq. (13a) satisfy the following relationship:

$$\begin{cases} 12kp^2\lambda_{\xi1}^8 + (p^2+3kp^{-2}+3k+1)\lambda_{\xi1}^6 - \dfrac{24}{625}kp^{-2}\lambda_{\xi1}^{12} \\ -\dfrac{3p^2+9kp^{-2}+9k+3}{625}\lambda_{\xi1}^{10} - 20p^{-2} = 0, \\ 4kp^2\lambda_{\xi2}^8 + (p^2 + \dfrac{kp^{-2}}{625} + \dfrac{k}{625} + 1)\lambda_{\xi2}^6 + k(1+p^{-2})\lambda_{\xi2}^2 \\ -\dfrac{8}{625}kp^2\lambda_{\xi2}^{12} - \dfrac{3}{625}(p^2+1)\lambda_{\xi2}^{10} + 4p^{-2} = 0. \end{cases} \tag{13b}$$

As shown in fig. 6, the energy generated in one cycle increases with the increasing of k. For example, the energy is 6.81 J/g, when $p = 1$, $k = 0.1$ and $X_2 = 17.5$; as p increases, the allowable working area of a harvester reduces and its stability declines. Moreover, the harvester will produce less energy too. As we know, the allowable area of an energy harvester decreases with the increase of the ratio between principal planar stretches p, together with the decrease of the structural stability and of the harvested energy. However, for the same nominal electrical displacement, the energy harvested in the structure will increase with increasing p and decreasing stretch. Hence, these two influential factors, decreasing allowable area and decreasing stretch, will decrease or increase the harvested energy. When $p = 0.5$, 0.9, 1, the ratio between principal planar stretches p has less influence compared with stretch λ. However, the ratio between principal planar stretches has more influence when $p = 1.1$ and $k = 0.1$.

From our previous research on the allowable area of a silicone rubber energy harvester, we proposed a stacking energy harvester and its performance test equipment, as shown in figs. 7 and 8. The stacking energy harvesters are emplaced separately in three sleeves, which are symmetrical around the axle wire as shown in figs. 7 and 8. These sleeves, the brace, upper and lower plates, are fixed with the floating body by a hinge bracket. An external load is applied on the energy harvester in each sleeve, and connected with the astral plate by swivel joints. A tie bar is connected with the central hinged support of the astral plate on the top, and the rigid wire at the bottom. The rigid wire passes through the central hole in the upper and lower plates, and is fastened at the bottom of the water on the other end.

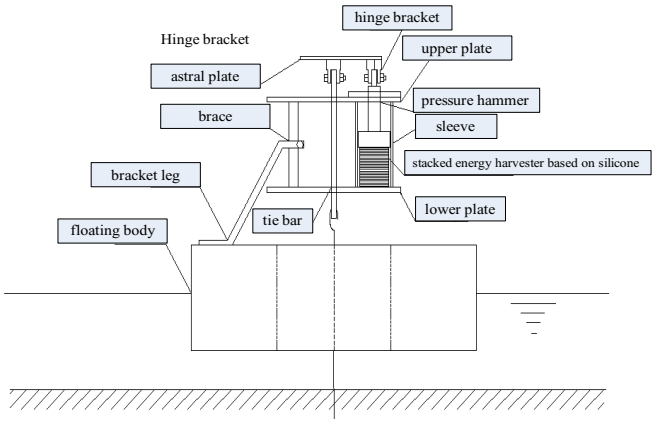

Fig. 7: (Color online) Energy harvester and its experimental setup.

Fig. 8: (Color online) Experimental setup for the energy harvester based on the silicone dielectric elastomer.

Figure 8 shows the configuration of energy harvester and its performance test device. The diameter of the silicone rubber film is 50 mm, the diameter and height of the electrode are 40 mm, and 60 mm, respectively. We use a plexiglas with a density of 1.8 g/cm^3 to form the main body of a collector and a hard aluminum alloy with a density of 2.8 g/cm^3 to prepare the carriages. When the motor drives the floating body to beat the water surface to produce waves, the energy harvester will endure a periodic mechanical force and accomplish the periodic conversion from mechanical to electric energy. There are 14 light-emitting diodes located in the device. Each diode has a

power of 0.06 W and the light lasts about 1.5 s, so the total amount of energy is 1.26 J and the energy density is 0.0036 J/g.

We studied the allowable area of a Mooney-Rivlin–type silicone rubber energy harvester under equal- and unequal-biaxial conditions, formulated the calculation method for the energy produced in one cycle, and gave the maximal energy of an energy harvester. The numerical results indicate that the allowable area increases when the ratio between principal planar stretches p and the material constant ratio k decrease. The periodic energy generated by a harvester increases as the parameter k increases, however, when the parameter p increases, the amount of energy is also influenced by $\lambda_{(3)}$. When $k = 0$ and $p = 1$, the result is identical to what is reported in Koh's conclusion. These results will provide significant assistance to the design and manufacture of a dielectric elastomer energy harvester.

REFERENCES

[1] Pelrine R., Kornbluh R., Pei Q. B. and Joseph J., *Science*, **287** (2000) 836.
[2] Brochu P. and Pei Q. B., *Macromol. Rapid Commun.*, **31** (2010) 10.
[3] O'Halloran A., O'Malley F. and McHugh P., *J. Appl. Phys.*, **104** (2008) 071101.
[4] Zhang H., Düring L., Kovacs G., Yuan W., Niu X. and Pei Q., *Polym Int.*, **59** (2010) 384.
[5] Gallone G., Carpi F., Rossi D., Levita G. and Marchetti A., *Mater. Sci. Eng. C*, **24** (2004) 555.
[6] Carpi F., Gallone G., Galantini F. and Rossi D., *Adv. Funct. Mater.*, **18** (2008) 235.
[7] Li B., Chen H., Wu J., Zhu Z., Xia D. and Jing S., *Proc. SPIE*, **7493** (2009) 74935S.
[8] Keplinger C., Kaltenbrunner M., Arnold N. and Bauer S., *Proc. Natl. Acad. Sci., U.S.A.*, **107** (2010) 4505.
[9] Wang H. M. and Xu Z. X., *Comput. Mater. Sci.*, **48** (2010) 440.
[10] Wang H. M., Ding H. J. and Chen Y. M., *Int. J. Solids Struct.*, **42** (2005) 85.
[11] Wang H. M. and Ding H. J., *Struct. Eng. Mech.*, **23** (2006) 525.
[12] Wang H. M. and Ding H. J., *Eur. J. Mech. A: Solids*, **25** (2006) 965.
[13] Wang H. M., Liu C.B. and Ding H. J., *Acta Mech. Sin.*, **25** (2009) 555.
[14] Wang H. M. and Chen W. Q., *Acta Mech. Solida Sin.*, **21** (2008) 536.
[15] Wang H. M. and Ding H. J., *J. Sound Vib.*, **307** (2007) 330.
[16] Wang H. M., Liu C. B. and Ding H. J., *Arch. Appl. Mech.*, **79** (2009) 753.
[17] Adrian Koh S. J., Zhao X and Suo Z, *Appl. Phys. Lett.*, **94** (2009) 262902.
[18] Zhao X. and Suo Z., *Appl. Phys. Lett.*, **91** (2007) 061921.
[19] Zhao X., Hong W. and Suo Z., *Phys. Rev. B*, **76** (2007) 134113.
[20] Suo Z., Zhao X. and Greene W. H., *J. Mech. Phys. Solids*, **56** (2008) 467.
[21] Zhou J., Hong W., Zhao X., Zhang Z. and Suo Z., *Int. J. Solids Struct.*, **45** (2008) 3739.
[22] Liu Y., Liu L., Zhang Z., Shi L. and Leng J., *Appl. Phys. Lett.*, **93** (2008) 106101.
[23] Zhao X. and Suo Z., *J. Appl. Phys.*, **101** (2008) 123530.
[24] Liu Y., Liu L., Leng J., Yu K. and Sun S., *Appl. Phys. Lett.*, **94** (2009) 211901.
[25] Díaz-Calleja, Riande E. and Sanchis M. J., *Appl. Phys. Lett.*, **93** (2008) 101902.
[26] Liu Y., Liu L., Zhang Z. and Leng J., *Smart Mater. & Struct.*, **18** (2009) 095024.
[27] Moscardo M., Zhao X., Suo Z. and Lapusta Y., *J. Appl. Phys.*, **104** (2008) 093503.
[28] Liu Y., Liu L., Sun S. and Leng J., *Smart Mater. & Struct.*, **18** (2009) 095040.
[29] Liu Y., Liu L., Sun S. and Leng J., *Polym. Int.*, **59** (2010) 371.
[30] He T., Zhao X. and Suo Z., *J. Appl. Phys.*, **106** (2009) 083522.
[31] Zhao X. and Suo Z., *Appl. Phys. Lett.*, **93** (2008) 251902.
[32] Zhao X. and Suo Z., *Appl. Phys. Lett.*, **95** (2009) 031904.
[33] Hong W., Zhao X. and Suo Z., *Appl. Phys. Lett.*, **95** (2009) 111901.
[34] Zhao Xuanhe and Suo Zhigang, *Phys. Rev. Lett.*, **104** (2010) 178302.
[35] Suo Z. and Zhu J., *Appl. Phys. Lett.*, **95** (2009) 232909.
[36] Zhu J., Cai S. and Suo Z., *Polym. Int.*, **59** (2010) 378.
[37] Liu Y., Sun S., Shi L. and Leng J., *Appl. Phys. Lett.*, **94** (2009) 096101.
[38] Carpi F., Raspopovic S., Frediani G. and Rossi D., *Polym. Int.*, **59** (2010) 422.
[39] Plante J. S. and Dubowsky S., *Int. J. Solids Struct.*, **43** (2006) 7727.
[40] Fox J. W. and Goulbourne N. C., *J. Mech. Phys. Solids*, **56** (2008) 2669.